Energy 220 (2021) 119710

Contents lists available at ScienceDirect

Energy

journal homepage: www.elsevier.com/locate/energy

Multi-well strategy for gas production by depressurization from methane hydrate-bearing sediments

M. Terzariol*, J.C. Santamarina

Earth Science and Engineering, KAUST, Thuwal, 23955-6900, Saudi Arabia

A R T I C L E I N F O

Article history:
Received 17 November 2019
Received in revised form
21 December 2020
Accepted 22 December 2020
Available online 26 December 2020

Keywords:
Multi-well
Hydrates
Gas production
Methane
Sediments
Energy

A B S T R A C T

Hydrate-bearing sediments are a potential source of energy. Depressurization is the preferred production method in mechanically stable and highly permeable sandy reservoirs. The goal of this study is to develop closed-form analytical solutions for multi-well depressurization strategies and to explore the synergistic interactions among wells. The key variables are the aquitard and sediment permeabilities, the reservoir layer and aquitard thicknesses, and water pressures in the far-field, at phase transformation and at the wells. These variables combine to define two governing dimensionless ratios (for permeability and fluid pressure), and a characteristic length scale λ_{sed}. Proposed solutions show that synergistic multi-well strategies dissociate a larger hydrate volume than an equal number of individual wells working independently. The optimal distance between wells increases: (1) with the length scale λ_{sed}, (2) for tighter aquitards, (3) for lower well pressure and when the original water pressure of the reservoir is close to the dissociation pressure, and (4) when both the aquitard and the reservoir are thick. Implications extend to both vertical and horizontal wells. The proposed closed-form solutions expedite design and economic analyses and allow the fast comparison of potential production scenarios.

1. Introduction

Methane hydrate is stable at relatively high pressure and low temperature. Seabed sediments host 95% of the hydrate mass; the rest is found in lakebed sediments and beneath the permafrost. Hydrate formation is pore-filling in coarse-grained sediments, while hydrate growth displaces the sediment grains to form nodules and lenses in fine-grained sediments [1].

The amount of methane gas trapped in hydrates could reach 1800 GtC ($1.8\text{x}10^{18}$ g of carbon [2]; – see also [3]). Hence, hydrate-bearing sediments are a potential source of energy. Suggested methods for gas production fall within three categories: *depressurization*, *thermal stimulation*, and *chemo-active methods*. The choice of production strategy depends on the reservoir characteristics, including the hydrate pore habit, effective stress, fines content, sediment permeability and compressibility. Depressurization is preferred in the case of pore-filling hydrate in high permeability sediments such as clean coarse sands. On the other hand, thermal stimulation is preferred in fine-grained sediments because of their low permeability, high gas entry pressure, and high compressibility [4,5]; during thermal stimulation, the hydrate volume expands 2 to 4 times as dissociation takes place across the phase boundary, and creates gas-driven 'fractures' that facilitate gas recovery [6–8]. However, thermal stimulation is energy demanding [9].

Chemo-active methods alter atomic interactions and free the methane molecule trapped in the clathrate structure. Chemical inhibitors shift the phase boundary in the P-T space to cause dissociation under the in-situ P-T conditions. A particularly attractive chemo-active technique is CO_2–CH_4 replacement, whereby the injected CO_2 replaces and releases the CH_4 as a guest molecule [10–12]. Replacement induces minimal stress changes and strains, however, this method requires pervious formations such as clean sands.

Field production pilot tests have been undertaken by the USA, Canada, Japan, and China. The test at the Mallik site in the Mackenzie Delta involved thermal stimulation and depressurization (Canada in 2002 and 2007/2008; [13,14]). The field production test by CO_2–CH_4 replacement in Ignik Sikumi trapped ~50% of the injected CO_2 in the formation (north slope, Alaska in 2011; [15]). Tests in the permafrost area of the Qilian Mountains combined depressurization and heating (China in 2011 and 2016; [16,17]). Japan conducted the first offshore test in the Nankai Trough in 2013

* Corresponding author.
E-mail addresses: marco.terzariol@kaust.edu.sa, mterza@gmail.com (M. Terzariol).

https://doi.org/10.1016/j.energy.2020.119710

followed by two production well tests in 2017; the successful tests lasted from 1-to-3 weeks [18,19]. The latest offshore production tests took place in the Shenhu Area of the South China Sea and involved controlled gas-liquid depressurization and enhanced screening strategies (offshore China – vertical well in 2017 and horizontal well in 2019/2020; [20,21]). Sand production issues have challenged field tests; while emphasis has been placed on screens, the interaction between vertical wells and the formation may cause tensile failure above the production zone and/or buckling collapse of screens within the production horizon [22].

Most of the current efforts and studies have involved depressurization. The low pressure field extends away from the well along conductive layers between aquitards. The maximum distance from the production well to the dissociation front depends on relative permeabilities (aquitard vs. reservoir), and the extent of depressurization relative to the dissociation pressure and the fluid pressure in the far-field. Simple analyses show that single independent wells cannot economically produce methane from known reservoirs at current oil prices [23,24].

Well-deployment strategies can significantly improve the affected volume. For example, single horizontal wells extend the dissociated volume linearly with the well length. Alternatively, we can consider multiple vertical wells for depressurization [24,25], thermal stimulation [26–28], and combined thermal-depressurization methods [29–31]. Unfortunately, studies conducted with complex multiphysics numerical simulators hide the interaction among the multiple variables involved and their relative importance, and there is no analytical solution available in the literature for multi-well scenarios.

The goal of this study is to develop closed-form analytical solutions for multi-well depressurization strategies and to explore synergistic interactions among wells. These solutions will allow us to optimize well configurations for specific reservoir characteristics and assess the reservoir volume engaged during depressurization.

2. Single and multi-well solutions

The analytical solutions developed herein apply at steady-state depressurization conditions when the dissociation boundary reaches the asymptotic size, ceases to expand and hydrate stops dissociating. At this moment, all produced water either leaks in through the aquitard layers or seeps in from the far field, and the pressure field reflects the distinct hydraulic conductivities in the hydrate-free sediment and the remaining hydrate bearing sediment. This asymptotic steady-state analysis does not capture the evolution of dissociation, but places emphasis on ultimate producible volumes.

For clarity and completeness, we present first the single-well production problem, addressed by the authors in a previous study [23]. Then, we extend the analysis to the multi-well problem to identify synergistic interactions between producing wells.

2.1. Single well production: vertical and horizontal solutions

Consider a single well in a leaky methane hydrate reservoir of thickness H bound between two aquitards layers of thickness b (Fig. 1). The dissociation front grows away from the well until the pressure field reaches steady-state conditions. At this point, only water flows into the well, and the pressure field exhibits a two-stage trend between the far field pressure u_{far}, the pressure at the phase boundary u* and the pressure at the well u_W (Fig. 1) The dissociation boundary terminal radius r* for a single vertical well results from mass conservation and equilibrium (Fig. 1-a [23]);

$$\left[B_{sed}\,K_1\left(\frac{r^*}{\lambda_{sed}}\right)-A_{sed}\,I_1\left(\frac{r^*}{\lambda_{sed}}\right)\right]=\left(u^*-u_{far}\right)\sqrt{\frac{k_{hbs}}{k_{sed}}}\,\frac{K_1\left(\frac{r^*}{\lambda_{hbs}}\right)}{K_o\left(\frac{r^*}{\lambda_{hbs}}\right)} \tag{1a}$$

where the characteristic lengths λ_{sed} and λ_{hbs} are functions of the reservoir geometry (H and b), the permeability of the sediment with hydrates k_{hbs} and after dissociation k_{sed}, and the permeability of the aquitards k'

$$\lambda_{sed}=\sqrt{\frac{k_{sed}}{k'}\,\frac{H\,b}{2}}\quad\text{and} \tag{1b}$$

$$\lambda_{hbs}=\sqrt{\frac{k_{hbs}}{k'}\,\frac{H\,b}{2}} \tag{1c}$$

The modified Bessel functions in Eq. (1a), (1b) and (1e) are $I_o()$ first kind and order zero, $I_1()$ first kind and first order, $K_o()$ second kind and order zero, and K_1 () second kind and first order. A_{sed} and B_{sed} parameters are:

$$A_{sed}=\frac{u^*-u_{far}}{I_o\left(\frac{r^*}{\lambda_{sed}}\right)}-\frac{B_{sed}\,K_o\left(\frac{r^*}{\lambda_{sed}}\right)}{I_o\left(\frac{r^*}{\lambda_{sed}}\right)} \tag{1d}$$

$$B_{sed}=\frac{u_W-u_{far}-\left(u^*-u_{far}\right)\dfrac{I_o\left(\frac{r_W}{\lambda_{sed}}\right)}{I_o\left(\frac{r^*}{\lambda_{sed}}\right)}}{K_o\left(\frac{r_W}{\lambda_{sed}}\right)-K_o\left(\frac{r^*}{\lambda_{sed}}\right)\dfrac{I_o\left(\frac{r_W}{\lambda_{sed}}\right)}{I_o\left(\frac{r^*}{\lambda_{sed}}\right)}} \tag{1e}$$

Similarly, the terminal distance x* for a single horizontal well drilled at mid height along the hydrate bearing layer is (Fig. 1-b):

$$\frac{\left[2\left(\frac{u_{far}-u_W}{u_{far}-u^*}\right)e^{\left(\frac{r_W-x^*}{\lambda_{sed}}\right)}-e^{\left(-2\frac{x^*-r_W}{\lambda_{sed}}\right)}-1\right]}{1-e^{\left(-2\frac{x^*-r_W}{\lambda_{sed}}\right)}}=\sqrt{\frac{k_{hbs}}{k_{sed}}} \tag{2}$$

2.2. Multi-well analytical solutions

Multiple neighboring wells interact with each other. Therefore, there must be an optimal inter well distance for a given reservoir and production conditions so that every point inside the depressurized zone is at or below the dissociation pressure u*. Let's analyze the cases of vertical and horizontal wells.

2.2.1. Multiple vertical wells

Consider an infinite number of vertical wells at a distance S from each other in a quincunx configuration (Fig. 2-a). Pumping lowers the pressure in all wells to u_W (at t = 0). Let's approximate the hexagonal geometry with a circle of diameter S. There is a pressure hump between wells; therefore, there is zero gradient and no flow across the imaginary boundary between wells at a distance ~ S/2.

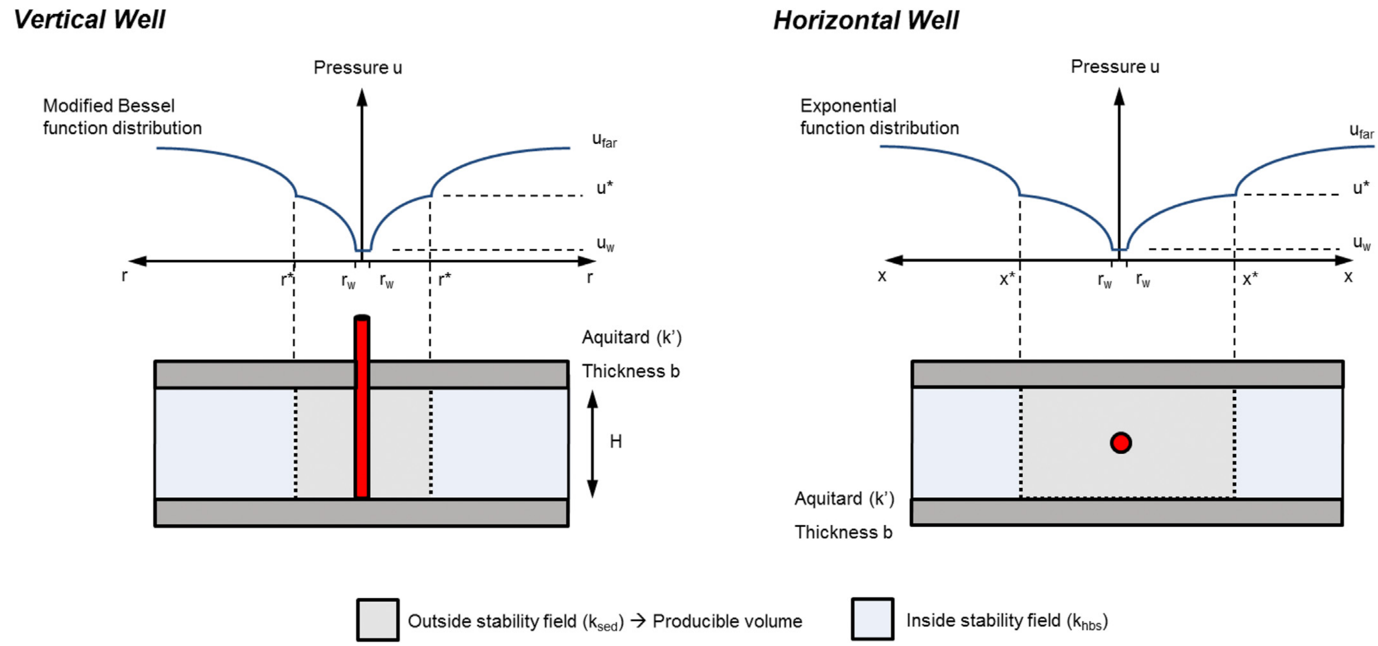

Fig. 1. Single well production. Water-pressure distribution due to depressurization in a hydrate bearing sediment layer bounded by top and bottom aquitards. The producible volume extends to radial distance r*. Variables involved: geometry (producible thickness H, aquitards thickness b, well radius r_w and either the radius r* or width x* of the produced zone), pressures (far field u_{far}, at phase transformation u* and at the well u_w), and permeabilities (hydrate-free sediment k_{sed}, hydrate bearing sediment k_{hbs} and aquitard layers k').

The axisymmetric pressure field u_r around a vertical well in a leaky aquifer with a no-flow boundary at $r = S/2$ is (details in Supplementary Material):

$$u_r = u_{far} + A\, I_o\left(\frac{r}{\lambda_{sed}}\right) + B\, K_o\left(\frac{r}{\lambda_{sed}}\right) \tag{3}$$

where the characteristic length λ_{sed} is defined in Eq. (1b). The following boundary conditions apply: (1) the pressure is $u_r = u_w$ at the well wall $r = r_w$, (2) the maximum pressure at the boundary $r = S/2$ is equal to the dissociation pressure $u_r = u^*$, and (3) the flow rate at the boundary $r = S/2$ is the leak-in from the top and bottom aquitards only, $q = q_{leak}$. Then, Equation (3) predicts the following pressure distribution:

$$u_r = u_{far} - \left[\frac{\left(u_w - u_{far}\right) K_o\left(\frac{S}{2\,\lambda_{sed}}\right) + \left(u_{far} - u^*\right) K_o\left(\frac{r_w}{\lambda_{sed}}\right)}{I_o\left(\frac{S}{2\,\lambda_{sed}}\right) K_o\left(\frac{r_w}{\lambda_{sed}}\right) - I_o\left(\frac{r_w}{\lambda_{sed}}\right) K_o\left(\frac{S}{2\,\lambda_{sed}}\right)}\right] I_o\left(\frac{r}{\lambda_{sed}}\right) + \left[\frac{\left(u_w - u_{far}\right) I_o\left(\frac{S}{2\,\lambda_{sed}}\right) + \left(u_{far} - u^*\right) I_o\left(\frac{r_w}{\lambda_{sed}}\right)}{I_o\left(\frac{S}{2\,\lambda_{sed}}\right) K_o\left(\frac{r_w}{\lambda_{sed}}\right) - I_o\left(\frac{r_w}{\lambda_{sed}}\right) K_o\left(\frac{S}{2\,\lambda_{sed}}\right)}\right] K_o\left(\frac{r}{\lambda_{sed}}\right) \tag{4}$$

2.2.2. Multiple horizontal wells

This case involves parallel wells drilled along the center of the hydrate-bearing layer, separated at a distance S from each other. Let's assume that the length of the well in the reservoir is much longer than the hydrate layer thickness $L \gg H$ (Fig. 2-b). Once again, the pressure field has a hump between wells and there is no horizontal flow across the plane between wells at a distance $x = S/2$. Then, the pressure distribution for horizontal wells in a leaky aquifer along the transverse well direction x is (details in Supplementary Material):

$$u_x = u_{far} + A\, e^{\left(\frac{x}{\lambda_{sed}}\right)} + B\, e^{\left(-\frac{x}{\lambda_{sed}}\right)} \tag{5}$$

where the characteristic length λ_{sed} is defined in Eq. (1b). We solve the pressure field for boundary conditions analogous to the vertical wells: $u_x = u_w$ at $x = r_w$, $u_x = u^*$ at $x = S/2$, and $q = q_{leak}$ at $x = S/2$. Then, the pressure distribution becomes:

$$u_x = u_{far} - \left(u_{far} - u^*\right) \frac{\sinh\left(\frac{x}{\lambda_{sed}}\right)}{\sinh\left(\frac{S}{2\,\lambda_{sed}}\right)} - \left(u_{far} - u_w\right) \frac{e^{\left(\frac{x - \frac{S}{2}}{\lambda_{sed}}\right)}\left[e^{\left(\frac{S-2x}{\lambda_{sed}}\right)} - 1\right]}{2\sinh\left(\frac{S}{2\,\lambda_{sed}}\right)} \tag{6}$$

Fig. 3 compares the pressure fields for single vertical and horizontal wells (Eqs. (1) and (2)) and well groups (Eqs. (4) and (6)) for the same reservoir and well pressure u_w. The optimal inter well separation S_{opt} is the maximum distance for complete dissociation of all hydrate between wells. Results highlight the synergistic interaction between wells in multi-well solutions.

2.3. Superposition: other multi-well configurations - optimal separation

The superposition method facilitates the analysis of optimal

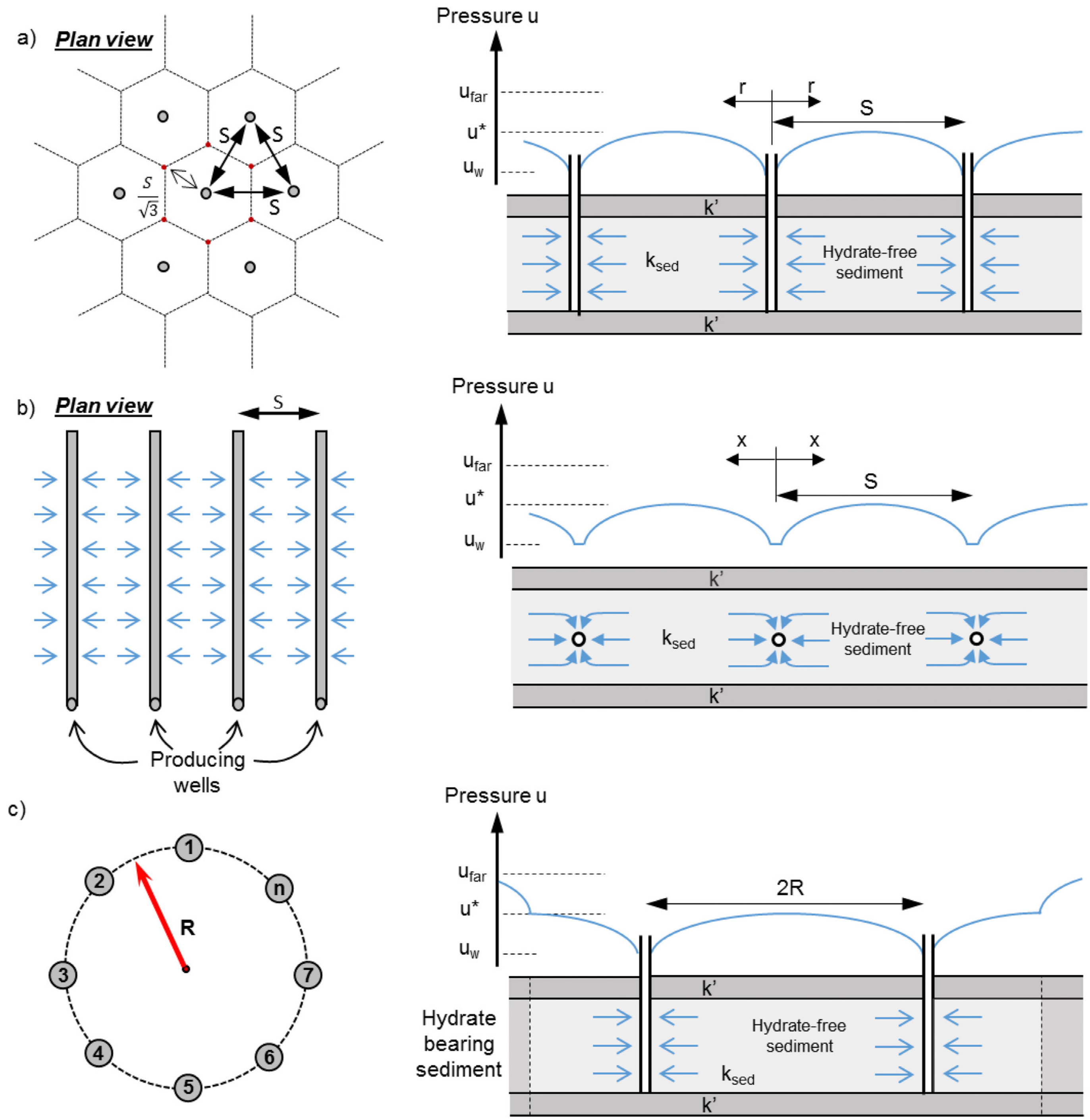

Fig. 2. Multi-well solutions. (a) Vertical wells in quincunx distribution forming equilateral triangles of side S. (b) Parallel horizontal wells distribution. (c) Vertical wells in circular distribution.

separation S_{opt} for more complex well configurations and variable depressurization strategies. In this approach, the pressure drawdown u_{far}-u_r at a given location is the sum of drawdowns contributed by all wells [32,33]. Let's use this method to obtain optimal separations for various configurations.

2.3.1. Vertical wells in quincunx configuration

Assume that all hydrate dissociates between wells. The pressure field around a single vertical well in a leaky aquifer without hydrate is obtained from Eq. (3) for boundary conditions: (1) $u_r = u_{far}$ at $r \rightarrow \infty$, and (2) $u_r = u_w$ at $r = r_w$:

$$u_r = u_{far} + \frac{u_w - u_{far}}{K_o\left(\frac{r_w}{\lambda_{sed}}\right)} K_o\left(\frac{r}{\lambda_{sed}}\right) \tag{7}$$

By considering immediate neighbors only, we obtain a first-order, lower-bound estimate of the optimal separation S_{opt} between wells in a quincunx configuration for equal u_w in all wells

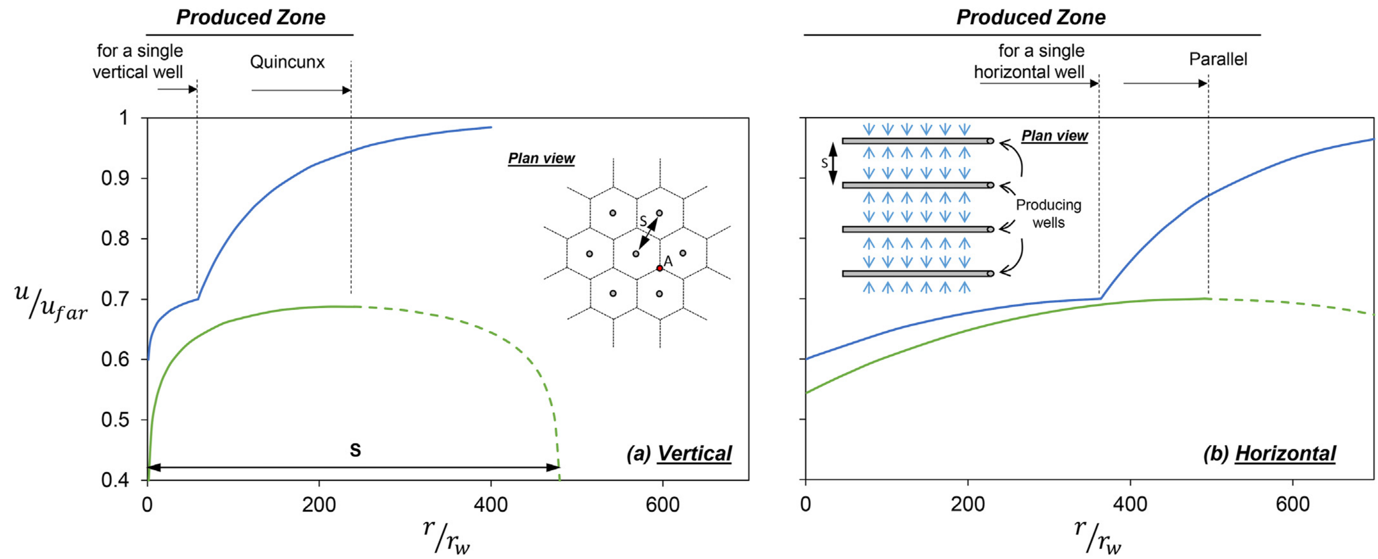

Fig. 3. Pressure distribution. (a) Vertical wells. (b) Horizontal wells. Solutions shown in blue for individual wells (equations in Ref. [23]) and in green for multi-well systems (Eqs. (4) and (6)). Parameters: u_{far} = 10 MPa, u_w = 6 MPa, u^* = 7 MPa, $k_{sed}/k' = 10^3$, and $k_{hbs}/k' = 10^2$.

(Note: the triple point "A" in Fig. 3-a is at distance $r = S_{opt}/\sqrt{3}$):

$$\frac{1}{3}K_o\left(\frac{r_w}{\lambda_{sed}}\right)=\frac{u_{far}-u_w}{u_{far}-u^*}\,K_o\left(\frac{S_{opt}}{\sqrt{3}\,\lambda_{sed}}\right) \tag{8}$$

where we assume that $u_r = u^*$ at the triple point. We can approximate Eq. (8) by:

$$S_{opt}=1.94\,\lambda_{sed}\left(\frac{\lambda_{sed}}{r_w}\right)^{\frac{1}{3}\left[\frac{u_{far}-u^*}{u_w-u_{far}}\right]}=1.94\,\lambda_{sed}\left(\frac{\lambda_{sed}}{r_w}\right)^{\frac{-1}{3U}} \tag{9a}$$

where the dimensionless pressure ratio U is

$$U=\frac{u_{far}-u_w}{u_{far}-u^*} \tag{9b}$$

2.3.2. *Vertical wells around a circle*

The drawdown at the center of the circle is n-times the contribution of each of the n wells, and it must reach the dissociation pressure u^*. If we assume all wells work at the same operational pressure u_w, the optimal radius R_{opt} for the circular array (Fig. 2-c) is obtained from:

$$\frac{1}{n}K_o\left(\frac{r_w}{\lambda_{sed}}\right)=\frac{u_{far}-u_w}{u_{far}-u^*}K_o\left(\frac{R_{opt}}{\lambda_{sed}}\right) \tag{10}$$

And, a first-order estimate of R_{opt} is:

$$R_{opt}=1.12\,\lambda_{sed}\left(\frac{\lambda_{sed}}{r_w}\right)^{\frac{1}{n}\left[\frac{u_{far}-u^*}{u_w-u_{far}}\right]}=1.12\,\lambda_{sed}\left(\frac{\lambda_{sed}}{r_w}\right)^{\frac{-1}{nU}} \tag{11}$$

2.3.3. *Horizontal wells in parallel configuration*

The pressure field for a horizontal well embedded in a leaky aquifer without hydrates is computed from Eq. (5) given boundary conditions: (1) $u_r = u_{far}$ at $x \to \infty$ and (2) $u_r = u_w$ at $x = r_w$ (details in Supplementary Material):

$$u_x=u_{far}+\left(u_w-u_{far}\right)e^{\left(\frac{r_w-x}{\lambda_{sed}}\right)} \tag{12}$$

The drawdown in the middle point between two horizontal wells is due to the two neighboring wells only. Then, assuming that the drawdown reaches the phase transformation pressure $u_{far} - u_x = u_{far} - u^*$ at the middle point between the two wells $x = S_{opt}/2$, the optimal separation S_{opt} for equal depressurization u_w at the wells is:

$$S_{opt}=2r_w+2\lambda_{sed}\,ln\left[\frac{1}{2}\left(\frac{u_{far}-u_w}{u_{far}-u^*}\right)\right]=2r_w+2\lambda_{sed}\,ln\left(\frac{U}{2}\right) \tag{13}$$

3. Results and discussion

The analytical solution for the vertical and horizontal single well problems show the interplay between permeabilities, fluid pressures and reservoir geometry. The predicted individual maximum size of the dissociation front agrees well with numerical results reported in the literature [23]. This section presents results for the multi-well configurations. In the absence of published solutions, we verified the global close form solution (Eqs. (4) and (6)) using the independent analysis based on the superposition method. Salient results are discussed next.

3.1. *Governing parameters*

A multi-well strategy dissociates a larger hydrate volume than an equal number of individual wells working independently (Fig. 3). Equations (9), (11) and (13) highlight the most important variables and their interplay in determining the optimal distance between wells in a multi-well solution. The key variables are the permeabilities of the sediment after hydrate dissociation k_{sed} and of the aquitard layers k', the reservoir and aquitard thicknesses H and b, and water pressures in the far-field u_{far}, at phase transformation

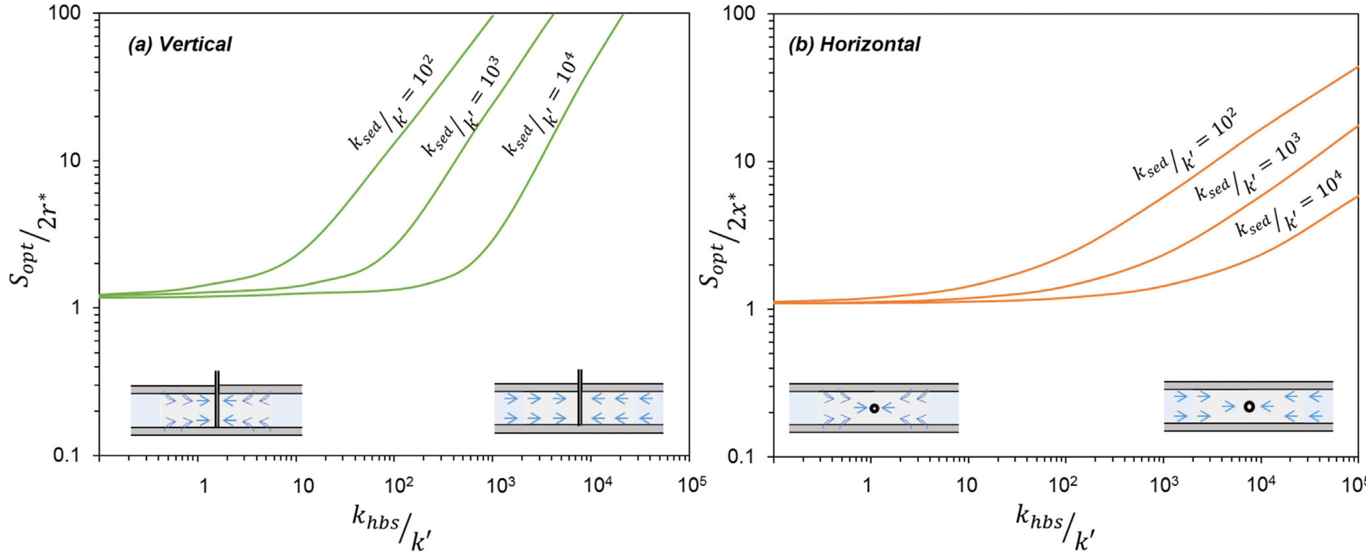

Fig. 4. Synergism in multi-well systems. Optimal distance S_{opt} compared to produced zone in single well solutions r* or x*. (a) Vertical wells in quincunx distribution. (b) Horizontal wells. For this example, $\frac{u_{far}-u_w}{u_{far}-u^*} = 1.6$. We use the superposition method to determine the ratio $S_{opt}/2r^*$ and $S_{opt}/2x^*$; the solution for the quincunx distribution, considers 12 neighboring wells.

u* and at the wells u_w. These variables combine to form two governing dimensionless ratios and a length scale:

$$K = \frac{k_{sed}}{k'} \tag{14}$$

$$U = \frac{u_{far} - u_w}{u_{far} - u^*} \tag{15}$$

$$\lambda_{sed} = \sqrt{\frac{k_{sed}}{k'} \frac{H\,b}{2}} \tag{16}$$

The optimal distance S_{opt} between wells increases: (1) with the length scale λ_{sed}, (2) for tighter aquitards, i.e. low k′, (3) for lower well pressure u_w, (4) when the original water pressure of the reservoir u_{far} is close to the dissociation pressure u*, and (5) when both the aquitard and the reservoir are thick, that is, large H·b.

Fig. 4 shows the benefits of multi-well solutions for vertical quincunx distribution and horizontal parallel configurations. There is synergetic interaction between wells when the optimal well separation S_{opt} exceeds the distance affected by a single vertical well $S_{opt} > 2r^*$ (Fig. 4-a) or a single horizontal well $S_{opt} > 2x^*$ (Fig. 4-b). Poor aquitards, $k_{hbs}/k' \rightarrow 1$, allow high transverse fluid influx and the pressure drop has a minimal effect on the hydrate layer; then the multi-well solution tends to be similar to multiple single wells, $S_{opt}/(2 \cdot r^*) \rightarrow 1$ and $S_{opt}/(2 \cdot x^*) \rightarrow 1$.

The analysis of interwell synergism in Fig. 4 involves the permeability of the hydrate-bearing sediment k_{hbs} because it affects the single well performance (r* and x*), yet k_{hbs} disappears in multi-well systems when all the hydrate mass dissociates between

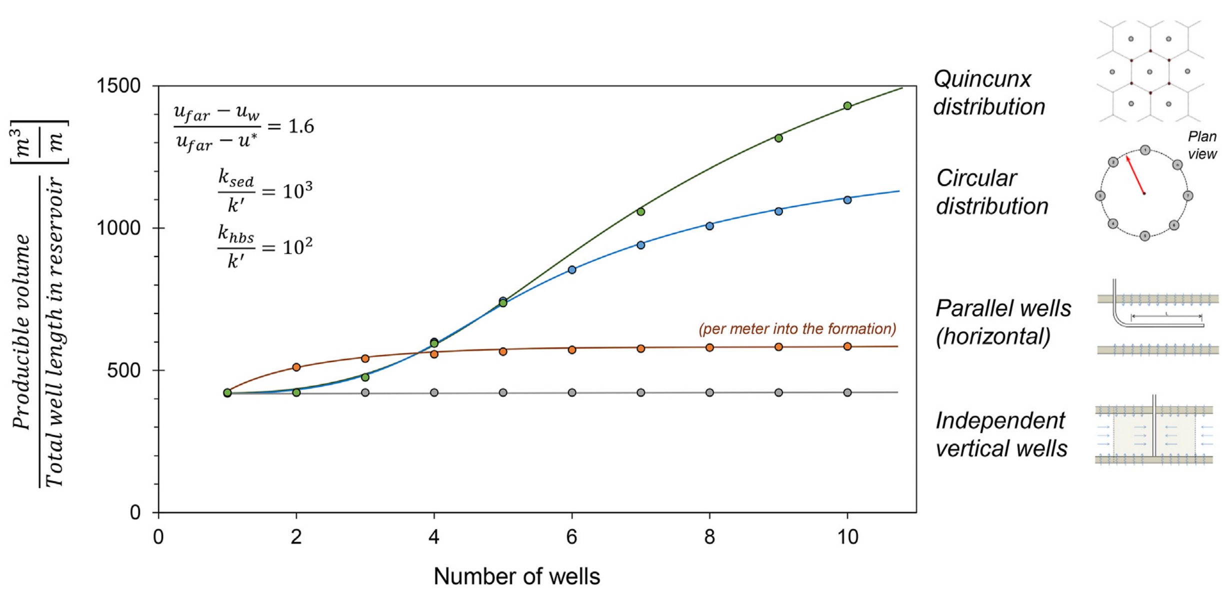

Fig. 5. Multi-well strategies: Producible volume normalized by the total length of all wells in the reservoir. Dimensionless parameters used in calculations: shown on the figure. Field specific dimensional variables: $r_w = 0.1$ m, H = 5 m, b = 1 m.

wells (Eqs. (4) and (6)). Then the counterintuitive impact of $K = k_{sed}/k'$ in Fig. 4 becomes clear: the size of the dissociation front r^* or x^* in single wells is sensitive to k_{hbs} while the separation S_{opt} in a multi-well strategy is not.

The sediment and aquitard hydraulic permeabilities k_{sed} and k' correspond to the end of dissociation and must take into account sediment compaction due to changes in effective stress, and relative permeability due to partial water saturation.

3.2. Field strategy

The single-well production strategy is uneconomical given today's technology and energy prices. Fig. 5 shows the benefits of multi-well strategies. The analysis assumes an effective well radius $r_w = 0.1$ m, a $H = 5$ m thick hydrate bearing layer bounded by two $b = 1$ m thick aquitards with a permeability ratios $k_{sed}/k' = 10^3$, $k_{hbs}/k' = 10^2$ and a pressure ratio $U = 1.6$. The vertical axis shows the producible reservoir volume normalized by the total length of wells in the reservoir.

Results for vertical wells show that the producible volume using optimal muli-well strategies can be several times higher than for the same number of wells working independently. Vertical wells in quincunx pattern are most effective. For the case analyzed in Fig. 5, 10 vertical wells in optimal quincunx configuration can produce a volume 3.5 times higher than 10 wells working independently; this configuration is applicable to accumulations with large areal distribution such as abyssal plains. The circular pattern of vertical wells is less efficient as they are involved in screening in-layer flow from the far field. This distribution might be suited for localized accumulations seen in mounds.

The synergism among parallel horizontal wells extends up to the first three wells: the two laterals screen far field flow and allow for a wider separation between internal wells. Most importantly, gas production from horizontal wells grows linearly with the well length within the reservoir L. Furthermore, horizontal wells avoid the costs associated with multiple raisers and seafloor manifolds, and are less sensitive to negative skin friction and well buckling within the production layer allowing for simpler well completions. Horizontal wells will benefit from elongated hydrate fields, as in continental slopes.

Multi-well hybrid solutions may include horizontal wells to delimit fields to be depressurized by vertical wells operating at different pressures. Such hybrid strategies can be easily analyzed using the superposition method described above.

4. Conclusions

Single-well gas production strategies from hydrate-bearing sediments are uneconomical. We developed closed-form analytical solutions for multi-well systems to analyze the benefits of synergetic interaction between wells.

Analytical solutions identify the governing variables: the permeabilities of the hydrate-free sediment and aquitard k_{sed} and k', the reservoir and aquitard thicknesses H and b, and the fluid pressures in the far field, at dissociation and at the well u_{far}, u^* and u_w. Their interplay is captured in dimensionless ratios K for permeability and U for fluid pressure, and the length scale λ_{sed}. The optimal separation between wells increases for thicker reservoirs bound by tighter aquitards, and when the initial reservoir pressure is similar to the dissociation pressure.

Optimal multi-well systems can dissociate a larger hydrate volume than an equal number of independent wells. The synergistic interaction among neighboring wells can significantly augment gas recovery and reduce production costs.

The two external wells in a set of parallel horizontal wells screen far-field flow and allow for higher separation among the internal wells in the set, thus, synergism extends up to the first three wells. The main advantage of horizontal wells is the linear increase in production volume with the well length within the reservoir L, reduce hardware costs, and simpler well completion.

Closed-form solutions can expedite the design and economic analyses and allow fast comparison of potential production scenarios.

Credit author statement

Both authors have contributed substantially to the manuscript and approved the final submission.

Declaration of competing interest

The authors declare that they have no known competing financial interests or personal relationships that could have appeared to influence the work reported in this paper.

Acknowledgments

Support for this research was provided by the KAUST endowment. G. E. Abelskamp edited this manuscript.

Appendix A. Supplementary data

Supplementary data to this article can be found online at https://doi.org/10.1016/j.energy.2020.119710.

References

[1] Dai S, Santamarina JC, Waite WF, Kneafsey TJ. Hydrate morphology: physical properties of sands with patchy hydrate saturation. J Geophys Res: Solid Earth 2012;117(B11).

[2] Ruppel CD, Kessler JD. The interaction of climate change and methane hydrates. Rev Geophys 2017;55:126–68. https://doi.org/10.1002/2016RG000534.

[3] Boswell R, Collett TS. Current perspectives on gas hydrate resources. Energy Environ Sci 2011;4(4):1206–15.

[4] Moridis GJ, Collett TS, Pooladi-Darvish M, Hancock S, Santamarina C, Boswell R, Kneafsey T, Rutqvist J, Kowalsky M, Reagan MT, Sloan ED. Challenges, uncertainties and issues facing gas production from gas hydrate deposits (No. LBNL-4254E). Berkeley, CA (US): Ernest Orlando Lawrence Berkeley National Laboratory; 2010.

[5] Jung JW, Jang J, Santamarina JC, Tsouris C, Phelps TJ, Rawn CJ. Gas production from hydrate-bearing sediments: the role of fine particles. Energy Fuels 2011;26(1):480–7.

[6] Jang J, Santamarina JC. Recoverable gas from hydrate-bearing sediments: pore network model simulation and macroscale analyses. J Geophys Res: Solid Earth 2011;116(B8).

[7] Jang J, Santamarina JC. Hydrate bearing clayey sediments: formation and gas production concepts. Mar Petrol Geol 2016;77:235–46.

[8] Shin H, Santamarina JC. Fluid-driven fractures in uncemented sediments: underlying particle-level processes. Earth Planet Sci Lett 2010;299:180–9.

[9] Moridis GJ, Sloan ED. Gas production potential of disperse low-saturation hydrate accumulations in oceanic sediments. Energy Convers Manag 2007;48(6):1834–49.

[10] Ersland G, Husebø J, Graue A, Kvamme B. Transport and storage of CO_2 in natural gas hydrate reservoirs. Energy Procedia 2009;1(1):3477–84.

[11] Jung JW, Espinoza DN, Santamarina JC. Properties and phenomena relevant to CH4-CO2 replacement in hydrate-bearing sediments. J. Geophy. Res. 2010;115:B10102. https://doi.org/10.1029/2009JB000812.

[12] Espinoza DN, Santamarina JC. P-wave monitoring of hydrate-bearing sand during CH_4–CO_2 replacement. Int J Greenh Gas Contr 2011;5(4):1031–8.

[13] Dallimore SR, Collett TS. Summary and implications of the Mallik 2002 gas hydrate production research well program. Sci Res Mallik 2002:1–36.

[14] Kurihara M, Sato A, Funatsu K, Ouchi H, Yamamoto K, Numasawa M, Ebinuma T, Narita H, Masuda Y, Dallimore SR, Wright F. January). Analysis of production data for 2007/2008 Mallik gas hydrate production tests in Canada. In: International oil and gas conference and exhibition in China. Society of Petroleum Engineers; 2010.

[15] Boswell R, Schoderbek D, Collett TS, Ohtsuki S, White M, Anderson BJ. The Ignik Sikumi field experiment, Alaska north slope: design, operations, and

implications for CO2−CH4 exchange in gas hydrate reservoirs. Energy Fuels 2017;31(1):140−53.
[16] Zhu Y, Zhang Y, Wen H, Lu Z, Jia Z, Li Y, Li Q, Liu Q, Wang P, Guo X. Gas hydrates in the qilian mountain permafrost, qinghai, northwest China. Acta Golog Sinica 2010;84(1):1−10.
[17] Li XS, Xu CG, Zhang Y, Ruan XK, Li G, Wang Y. Investigation into gas production from natural gas hydrate: a review. Appl Energy 2016;172:286−322.
[18] Yamamoto K, Terao Y, Fujii T, Ikawa T, Seki M, Matsuzawa M, Kanno T. Operational overview of the first offshore production test of methane hydrates in the Eastern Nankai Trough. In: Offshore technology conference. Offshore Technology Conference; 2014.
[19] Yamamoto K, Wang XX, Tamaki M, Suzuki K. The second offshore production of methane hydrate in the Nankai Trough and gas production behavior from a heterogeneous methane hydrate reservoir. RSC Adv 2019;9(45):25987−6013.
[20] Li JF, Ye JL, Qin XW, Qiu HJ, Wu NY, Lu HL, Xie WW, Lu JA, Peng F, Xu ZQ, Lu C. The first offshore natural gas hydrate production test in South China Sea. China Geol 2018;1(1):5−16.
[21] Ye JL, Qin XW, Xie WW, Lu HL, Ma BJ, Qiu HJ, Liang JQ, Lu JA, Kuang ZG, Lu C, Liang QY. The second natural gas hydrate production test in the South China Sea. China Geol 2020;3(2):197−209.
[22] Shin H, Santamarina JC. Sediment-well interaction during gas production from hydrate bearing sediments: hydro-mechanical coupling and implications. Acta Geotechnica 2016;12:883−95.
[23] Terzariol M, Goldsztein G, Santamarina JC. Maximum recoverable gas from hydrate-bearing sediments by depressurization. Energy 2017;141:1622−8.
[24] Moridis GJ, Reagan MT, Queiruga AF, Boswell R. Evaluation of the performance of the oceanic hydrate accumulation at site NGHP-02-09 in the Krishna-Godavari Basin during a production test and during single and multi-well production scenarios. Mar Petrol Geol 2019;108:660−96. https://doi.org/10.1016/j.marpetgeo.2018.12.001.
[25] Sun Z, Xin Y, Sun Q, Ma R, Zhang J, Lv S, Cai M, Wang H. Numerical simulation of the depressurization process of a natural gas hydrate reservoir: an attempt at optimization of field operational factors with multiple wells in a real 3D geological model. Energies 2016;9(9):714.
[26] Li G, Li XS, Li B, Wang Y. Methane hydrate dissociation using inverted five-spot water flooding method in cubic hydrate simulator. Energy 2014;64: 298−306.
[27] Wang Y, Li XS, Li G, Zhang Y, Li B, Chen ZY. Experimental investigation into methane hydrate production during three-dimensional thermal stimulation with five-spot well system. Appl Energy 2013;110:90−7.
[28] Wang Y, Feng JC, Li XS, Zhang Y. Experimental investigation of optimization of well spacing for gas recovery from methane hydrate reservoir in sandy sediment by heat stimulation. Appl Energy 2017;207:562−72.
[29] Song Y, Cheng C, Zhao J, Zhu Z, Liu W, Yang M, Xue K. Evaluation of gas production from methane hydrates using depressurization, thermal stimulation and combined methods. Appl Energy 2015;145:265−77.
[30] Feng JC, Wang Y, Li XS. Hydrate dissociation induced by depressurization in conjunction with warm brine stimulation in cubic hydrate simulator with silica sand. Appl. energy 2016;174:181−91.
[31] Wang Y, Feng JC, Li XS, Zhang Y. Influence of well pattern on gas recovery from methane hydrate reservoir by large scale experimental investigation. Energy 2018;152:34−45.
[32] Reilly TE, Franke OL, Bennett GD. The principle of superposition and its application in ground-water hydraulics: techniques of Water-Resources Investigations of the United States Geological Survey. 1987. Chapter B6.
[33] Bear J. Hydraulics of groundwater. New York: Dover Publications Inc. Mineola; 2012.